Subpicosecond Midinfrared Spectroscopy of the P_{fr} Reaction of Phytochrome Agp1 from *Agrobacterium tumefaciens*

Christian Schumann,* Ruth Groß,* Matthias M. N. Wolf,* Rolf Diller,* Norbert Michael,† and Tilman Lamparter†
*Fachbereich Physik, Technische Universität Kaiserslautern, Kaiserslautern, Germany; and †Institut für Pflanzenphysiologie, Freie Universität Berlin, Berlin, Germany

ABSTRACT Phytochromes are light-sensing pigments found in plants and bacteria. For the first time, the P_{fr} photoreaction of a phytochrome has been subject to ultrafast infrared vibrational spectroscopy. Three time constants of 0.3 ps, 1.3 ps, and 4.0 ps were derived from the kinetics of structurally specific marker bands of the biliverdin chromophore of Agp1-BV from *Agrobacterium tumefaciens* after excitation at 765 nm. VIS-pump-VIS-probe experiments yield time constants of 0.44 ps and 3.3 ps for the underlying electronic-state dynamics. A reaction scheme is proposed including two kinetic steps on the S_1 excited-state surface and the cooling of a vibrationally hot P_{fr} ground state. It is concluded that the upper limit of the *E-Z* isomerization of the $C_{15} = C_{16}$ methine bridge is given by the intermediate time constant of 1.3 ps. The reaction scheme is reminiscent of that of the corresponding P_r reaction of Agp1-BV as published earlier.

INTRODUCTION

In plants and bacteria, a multitude of processes is controlled by phytochromes (1,2), a class of photoreceptor proteins with two photochemically interconvertible and thermally stable states P_r and P_{fr} that absorb in the red and far-red spectral region, respectively. This feature of phytochromes not only allows the investigation of two different reactions of the same chromophore within one binding environment, but also makes them prototypes for biomimetic bistable light-driven switches. Three-dimensional structures of the chromophore-binding environments of bacterial phytochromes, DrBphP (3,4) and RpBphP3 (5), have recently been resolved.

The primary processes of the two photoconversions involve a *Z-E* isomerization of the methine bridge between rings C and D of the bilin chromophore for the P_r reaction and an *E-Z* isomerization for the P_{fr} reaction (6,7). Each reaction pathway involves several intermediate states, with the first ones being lumi-R (P_r reaction) and lumi-F (P_{fr} reaction), which are formed quickly after photoexcitation. The following reaction steps occur on the microsecond to millisecond timescale and have been characterized by UV/VIS, FTIR, and resonance Raman (RR) spectroscopy using low-temperature trapping techniques (8–15). In all bacterial and plant phytochromes known so far, the relatively slow P_r photoreaction takes place within ~5–100 ps as opposed to the relatively fast P_{fr} photoreaction which occurs on the timescale of a few picoseconds (16–18).

The primary photoreaction of the P_r form of different members of the phytochrome family has been subject to numerous investigations, including ultrafast VIS-VIS (17–22) and VIS-IR (23,24) pump-probe as well as fluorescence (25–27) spectroscopy. In contrast, the literature on the primary processes of the P_{fr} reaction is still very scarce. However, the high rate of its excited electronic-state decay has been quantified by ultrafast VIS-VIS spectroscopy (16–18). Further, fluorescence studies on the P_{fr} form of oat phytochrome do not show any detectable fluorescence (26), in line with a very efficient quenching of the excited electronic state.

In this work, we address the primary photoreaction of the P_{fr} form of the biliverdin-binding phytochrome Agp1 (Fig. 1) from *Agrobacterium tumefaciens* (28) by ultrafast mid-IR transient absorption spectroscopy. To our knowledge, this is the first ultrafast IR investigation of the P_{fr} reaction of a member of the phytochrome family. Details of the chromophore-protein interaction in Agp1-BV have already been obtained by site-directed mutagenesis and mass spectrometry, showing the covalent binding of the biliverdin (BV) chromophore via its ring A-vinyl side chain to the Cys^{20} residue (29). In both stable states, P_r and P_{fr}, the chromophore has been found protonated via RR spectroscopy and flash photolysis experiments (30). Recent results using locked bilin chromophores (31,32) suggest that the chromophore configuration is *ZZZssa* in P_r and *ZZEasa* in P_{fr} (*ZZZssa* and *ZZEasa* denote the configuration (*Z*, *E*) and conformation (*a*, *s*) of the methine bridges in the order A-B, B-C, and C-D).

As has been demonstrated earlier (34,35), ultrafast mid-IR spectroscopy is an excellent method to monitor light-induced structural dynamics. Here, it allows us to follow the transient vibrational spectra of the molecular states along the primary P_{fr} photoisomerization in Agp1-BV with subpicosecond time resolution. Combined with the electronic-states dynamics as obtained by transient absorption measurements in the visible spectra, different reaction models for the primary P_{fr} reaction can be evaluated.

Submitted August 9, 2007, and accepted for publication December 3, 2007.

Address reprint requests to Rolf Diller, Tel.: 49-631-205-2323; E-mail: diller@physik.uni-kl.de.

Tilman Lamparter's present address is Universität Karlsruhe, Botanik 1, D-76128 Karlsruhe, Germany.

Editor: Feng Gai.

0006-3495/08/04/3189/09 $2.00

doi: 10.1529/biophysj.107.119297

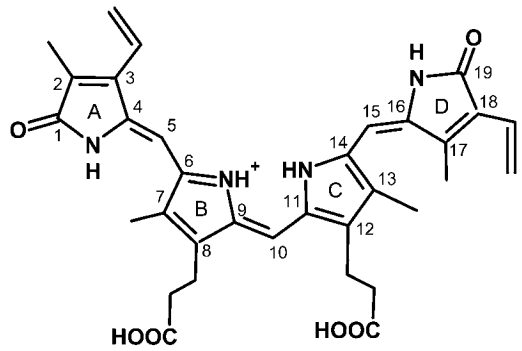

FIGURE 1 Chemical structure of the biliverdin (BV) chromophore in *ZZEasa* configuration, as suggested for the P_{fr} state (31).

METHODS

Sample preparation

Agp1 from *Agrobacterium tumefaciens* was expressed and purified as already described elsewhere (28). A D_2O (pD = 7.8) buffer solution (20 mM Tris, 50 mM NaCl) was used for all experiments. The protein was concentrated by ultrafiltration (YM-50, Centricon, Houston, TX) to a viscous smear, homogeneously spread on a 1.5-inch-diameter CaF_2 window (2 mm thick) and sealed by a second, similar window. In the absorption maximum of the P_r form at $\lambda_{max} = 700$ nm, the optical density of the sample was between ~0.5 OD and ~1.0 OD, equivalent to a pathlength of ~25–50 μm. This translates to an optical density of ~2 in the amide I/II-region of the steady-state FTIR spectrum of the sample. Note that the photoinduced IR-difference signals (see discussion below) are three orders-of-magnitude smaller (~1 mOD). To allow experiments in the region of high amide I background absorption, samples of lower optical density were used.

The sample was rotated and moved in the focus plane of the laser beam perpendicular to the direction of incidence during the experiment to provide fresh sample conditions for each laser pulse, i.e., to exchange the (microscopic) excited sample volume between two pump-and-probe events (1.6 ms) and to allow for sufficient recovery of the P_{fr} state. To avoid photoproduct buildup, firstly an excitation wavelength of $\lambda_{exc} = 765$ nm on the red edge of the P_{fr} absorption band was chosen. Secondly, the sample was irradiated by background light from a halogen lamp (K2500-LCD, red filter, Schott, Mainz, Germany), fitting the absorption spectrum of the P_r form ($\lambda_{max} = 700$ nm). All measurements were performed at room temperature. Sample integrity was confirmed by static FTIR and UV/VIS spectroscopy before and after the experiments. Except for general bleaching of the steady-state absorption in the visible up to ~10% until the sample was discarded, no spectral changes were observed.

Pump-probe spectrometer

The short laser pulses for the pump-probe spectrometer were generated in nonlinear optical devices. A Ti:Sa-regenerative amplifier system (CPA 2001, Clark-MXR, Dexter, MI) was used as pump source for the whole experiment. The visible pump pulses were generated in a homebuilt noncollinear optical parametric amplifier (NOPA), yielding pulses tunable between 470 and 765 nm with pulse lengths routinely at 60 fs.

Infrared probe pulses were generated in a two-stage optical parametric amplifier with subsequent difference frequency mixing. The center wavelength of the probe pulses is tunable between 800 cm^{-1} and 2500 cm^{-1} (36). After passing through the sample, the probe pulses with a typical full width at half-maximum (FWHM) of 100 cm^{-1} are dispersed in a polychromator and detected by a 32-element MCT array (Infrared Systems Development, Winter Park, FL), comprising a spectral window of ~300 nm (≈90 cm^{-1} at 1750 cm^{-1} and ≈40 cm^{-1} at 1180 cm^{-1}). The pump beam was chopped at 318 Hz (half the laser repetition rate), and pump-induced absorption differences were evaluated on a single-shot basis. Control measurements on a thin silicon wafer were performed before and after each experiment to determine the time zero and the FWHM of the instrument response function (typically 280 fs). The optical path through the front CaF_2 window and other parameters were identical to those of the phytochrome measurements. The spectral resolution, which varies slightly with the probe wavenumber, was typically 2.5 cm^{-1}.

For VIS-VIS pump-probe experiments, the same NOPA was used as pump source, and the probe pulses were generated by a second NOPA. The chopping scheme was the same as in VIS-IR experiments. After passing through the sample, the probe pulses (spectral width ~20 nm) were dispersed by a monochromator (bandwidth 6 nm) and detected by a photodiode. Time zero and FWHM of the system response (100 fs) were determined by cross correlation in a BBO crystal or in a SiC-photodiode (two-photon absorption (37)).

The recorded data are the pump-induced absorbance changes $\Delta A(\Delta t, \lambda_{pr})$; cuts along the time axis (Δt) are transients for fixed wavenumbers; and cuts along the probe wavenumber axis (λ_{pr}) are difference spectra at discrete delay times. The broadband IR probe pulses along with the detector array allow the detection of one spectral window at a given center wavelength (see above). Comparability and normalization of the IR data within the entire investigated spectral regions (Figs. 2 and 3) was achieved via sufficient overlap between adjacent spectral windows.

Negative absorbance changes display the disappearance of IR absorption and thus depopulation of the P_{fr} electronic ground-state vibrations (bleach bands). Positive absorbance changes indicate the absorption of newly populated vibrational states.

The obtained absorbance changes $\Delta A(\Delta t, \lambda_{pr})$ between 0.4 ps and 50 ps were analyzed by a global multiexponential fit,

$$\Delta A(\Delta t, \lambda_{pr}) = A_0(\lambda_{pr}) + \sum_{i=1}^{N} A_i(\lambda_{pr}) \times \exp\left(-\frac{\Delta t}{\tau_i}\right), \quad (1)$$

with $A_0(\lambda_{pr})$ being the pump-induced absorption changes for $\Delta t \rightarrow \infty$ and $A_i(\lambda_{pr})$ being the decay associated spectra (DAS) of the corresponding time constants τ_i.

RESULTS

Transient IR absorption spectra of Agp1-BV after photoexcitation at $\lambda_{exc} = 765$ nm were recorded for the carbonyl and

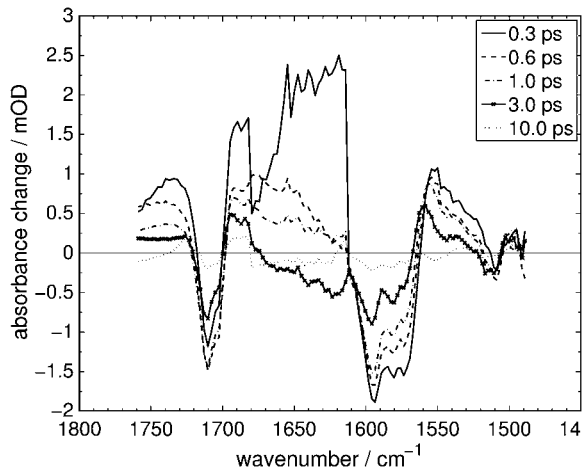

FIGURE 2 Difference spectra of the carbonyl and ethylenic stretch regions of Agp1-BV P_{fr} after excitation at $\lambda_{exc} = 765$ nm at selected delay times.

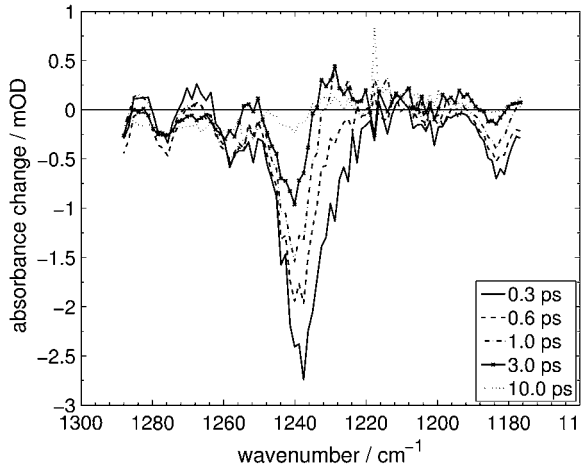

FIGURE 3 Difference spectra of the fingerprint region of Agp1-BV P_{fr} after excitation at $\lambda_{exc} = 765$ nm at selected delay times.

ethylenic stretch regions (1490–1760 cm^{-1}) and the fingerprint region (1177–1288 cm^{-1}). Difference spectra in the respective spectral regions at various delay times are depicted in Figs. 2 and 3. To correlate the transient vibrational signals (Fig. 4) with the electronic-state dynamics, ultrafast VIS-VIS pump-probe experiments were conducted on the same samples, with excitation at 765 nm and probing at 630, 655, 680, 705, 730, and 755 nm (see Fig. 5 for representative transients).

Band assignment

The structural dynamics of the biliverdin chromophore are monitored by the temporal evolution of vibrational marker

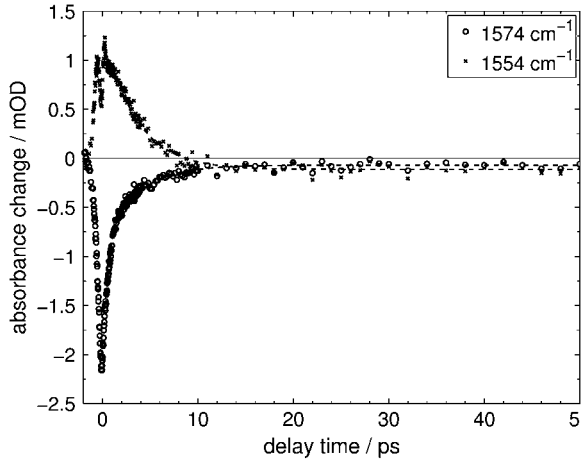

FIGURE 4 Transient absorption changes of Agp1-BV P_{fr} after excitation at $\lambda_{exc} = 765$ nm at selected probe wavenumbers of 1554 cm^{-1} and 1574 cm^{-1}. (*Dashed line*) Global fit with time constants of $\tau_1 = 0.3 \pm 0.1$ ps, $\tau_2 = 1.3 \pm 0.1$ ps, and $\tau_3 = 4.0 \pm 0.1$ ps. For the fit, only data after 400 fs delay time was used to exclude nonlinear artifacts before (perturbed free induction decay (57)) and at time zero (cross phase modulation (58)) as well as the system response.

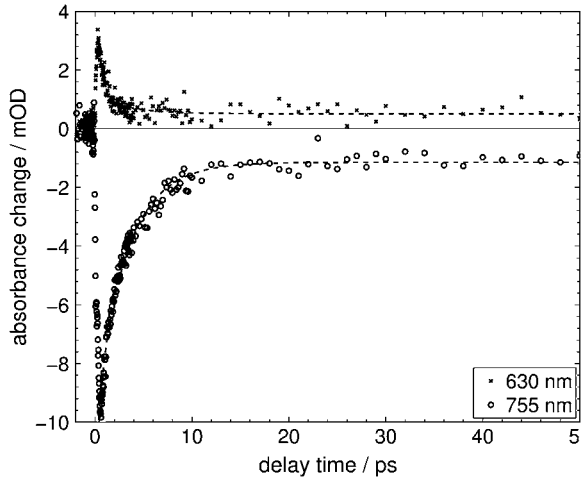

FIGURE 5 Transient absorption changes of Agp1-BV P_{fr} after excitation at $\lambda_{exc} = 765$ nm at selected probe wavelengths of 630 nm and 755 nm. (*Dashed line*) Global fit with time constants of $t_{V1} = 0.44$ pm 0.05 ps, and $t_{V2} = 3.3$ pm 0.1 ps. Data before 400 fs delay time was excluded from the fit.

bands. The timescale of the detected absorbance changes and the fact that the most significant structural changes are to be expected from the chromophore strongly suggest an assignment of the detected signals to vibrations of the BV chromophore rather than the protein moiety. Taking into account results from experiments using locked chromophores (31,32), we base our band assignment on the commonly accepted assumption that the chromophore structure of the P_{fr} form is *ZZEasa*. In support of the literature-based assignments, density functional theory (B3LYP/6-31G**) frequency calculations (38) on the *ZZEasa* chromophore were performed. For the calculations, all pyrrole nitrogens were modeled as protonated (30), no counterion was used, and vibrational frequencies were scaled with a global factor of 0.9613 (39).

In the carbonyl stretch region (see Fig. 2), the instantaneous bleach band at 1710 cm^{-1} is assigned to the $C_{19} = O$ stretching vibration, based on the results in the literature (9,10,40) and our own calculations. The hydrogen bonding of the ring D carbonyl group to His^{280} (3,15) lowers its stretching frequency significantly, whereas the ring A carbonyl group is not hydrogen-bonded and shows up at higher wavenumbers in PhyA-PΦB (10). Furthermore, since the isomerization occurs at the methine-bridge linking rings C and D, the contribution of modes located on ring D to the difference spectra can be expected to be substantially larger.

The manifold of bleach bands with peaks at 1594 cm^{-1}, 1580 cm^{-1}, and 1574 cm^{-1} can be assigned to C=C stretching vibrations of the π-system comprised by the pyrrole rings and the linking methine bridges. Previous FTIR experiments on isotope-labeled Cph1-PCB (40), as well as RR experiments on Agp1-BV (30) and PhyA-PΦB (13,14), and FTIR experiments on PhyA-PΦB (9) have found these bands and assigned them to C=C stretching modes. In addition,

our own calculations show a multitude of modes with dominant C=C stretching character in this spectral region.

Two pyrrole breathing modes located mainly on rings B and C are favored for the assignment of the small bleach band at 1509 cm^{-1}. The frequencies of these two modes were calculated to 1491 cm^{-1} and 1523 cm^{-1}. The involvement of their constituent atoms in the delocalized π-system of the chromophore backbone makes them sensitive to the isomerization.

The broad and short-lived positive signal between 1610 cm^{-1} and 1700 cm^{-1} appears almost instantaneously and decays with a time constant of 0.3 ps (see analysis below, Fig. 6). Thus, it is likely due to S_1 vibrational modes.

In the fingerprint region, our own calculations show numerous C-H rocking and C-C stretching vibrations, so that the assignment of the difference bands in Fig. 3 at 1276 cm^{-1}, 1238 cm^{-1} and 1184 cm^{-1} to modes of that character is only qualitative.

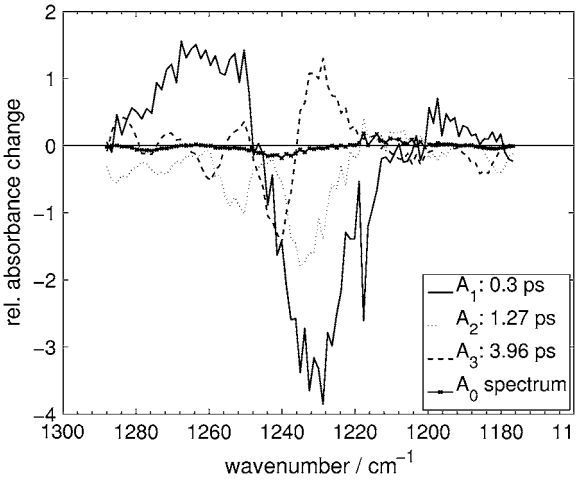

FIGURE 7 Decay-associated spectra for the P_{fr} primary reaction of Agp1-BV in the fingerprint region as derived from a global fit.

Kinetic analysis

A global analysis of the complete time-resolved IR data was performed via Eq. 1. Three exponentials are necessary to fit the data, whereas a four-exponential approach does not increase the goodness of fit. This analysis yields time constants of $\tau_1 = 0.3 \pm 0.1$ ps, $\tau_2 = 1.3 \pm 0.1$ ps, and $\tau_3 = 4.0 \pm 0.1$ ps, and the corresponding decay-associated spectra (DAS) A_1, A_2 and A_3, as shown in Figs. 6 and 7 for the respective spectral regions. Singular value decomposition of the time-resolved difference spectra and triexponential fit of the most significant component (not shown) renders time constants of 0.3 ps, 1.0 ps, and 3.6 ps. This further corroborates the results of the global fit.

The further discussion will make significant use of the shapes of the DAS, whose features can be compiled as follows (note that negative/positive amplitudes of the DAS represent absorbance strength, which increases/decreases with the respective time constants): A_1 shows signals that appear within the system response time of the experiment, thus positive signals are interpreted as signals from the first states detectable by the experiment. The short-lived and broad absorption bands centered at ~1740 cm^{-1}, 1650 cm^{-1}, and 1265 cm^{-1} are then likely to be caused by S_1 vibrational modes that are formed rapidly after photoexcitation. The negative contributions in A_1 at ~1563 cm^{-1} and 1230 cm^{-1}, together with its local minimum at ~1697 cm^{-1}, do not show any significant overlap with the ground-state bleach signals at 1710 cm^{-1}, 1594 cm^{-1}, and 1238 cm^{-1}, but are systematically red-shifted. Furthermore, they show a systematic overlap with negative contributions of A_2 and positive contributions of A_3, suggesting that A_1 and A_2 represent processes that feed a state related to A_3. In the context of the described systematics, it is plausible to regard the local minimum of A_1 at 1697 cm^{-1} as a negative contribution in A_1, in line with those at 1563 cm^{-1} and 1230 cm^{-1}, since the broad positive S_1-absorption in A_1 can easily obscure negative bands.

On the other hand, the negative contributions of A_3 coincide well with the most prominent ground-state bleach signals at 1710 cm^{-1}, 1594 cm^{-1}, and 1238 cm^{-1}, in addition to further minor bleach signals at 1511 cm^{-1}, 1277 cm^{-1}, 1260 cm^{-1}, and 1186 cm^{-1}. Overall, A_3 shows a shape that is typical for vibrational cooling, with negative contributions overlapping with ground-state absorption bands, and positive contributions that are systematically red-shifted and asymmetrically broadened to the red side of the spectrum. Such characteristic patterns have been observed with transient IR spectroscopy on azobenzene (41) and protonated Schiff base retinal in solution (42) and have been attributed to vibrational cooling in the electronic ground state. Similar processes have been reported for many molecular systems in the condensed phase (43). The time constant τ_3 in our experiment complies

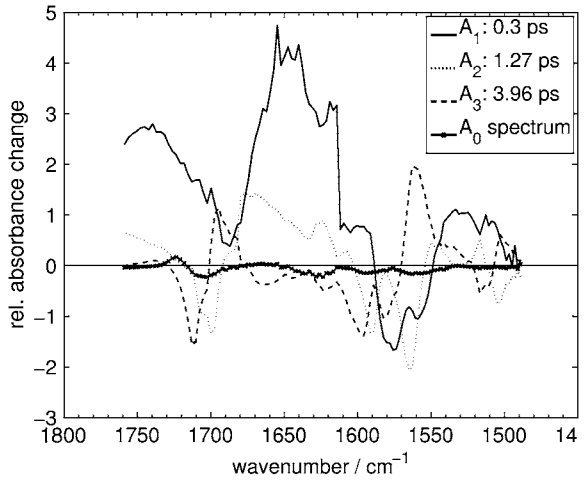

FIGURE 6 Decay-associated spectra for the P_{fr} primary reaction of Agp1-BV in the carbonyl and ethylenic stretch regions as derived from a global fit.

with the time range found for electronic ground-state vibrational cooling in protein systems (24,34,44).

The A_0 spectra of the global analysis of the infrared data represent the residual signals for virtually infinite delay time, and thus should show the difference spectra of lumi-F–P_{fr}. Although the low isomerization quantum yield (see below) hampers the identification of lumi-F in the A_0 spectrum, qualitative agreement is found between the A_0-carbonyl region and low-temperature FTIR difference spectra of PhyA-PΦB (9,10).

From the transient absorption experiments in the visible with probe wavelengths of 630, 655, 680, 705, 730, and 755 nm, two global time constants of $\tau_{V1} = 0.44 \pm 0.05$ ps and $\tau_{V2} = 3.3 \pm 0.1$ ps were derived. Singular-value decomposition analysis as well yields two time constants of 0.6 ps and 3.3 ps, in good agreement with the global fit results. The transients given in Fig. 5 show the recovery of the electronic ground-state bleach ($\lambda_{max} \approx 750$ nm), which is probed at 755 nm, and the decay of the S_1 excited-state absorption, which is probed at 630 nm and which accompanies the ground-state bleach decay. It should be kept in mind that the P_{fr} state of Agp1-BV exhibits significant absorbance between 600 and 800 nm (28). The traces at both wavelengths show contributions from both detectable time constants τ_{V1} and τ_{V2}, whereas the amplitude of τ_{V2} is substantially larger for the recovery of the ground-state bleach compared to the excited-state absorption decay. The contribution of the τ_{V2} component in the transient signal at 630 nm is considered due to ground-state processes (see below).

The relative amount of recovery of the initial ground-state bleach signals in the IR allows the determination of the isomerization quantum yield independently of a specific reaction scheme (24). For this purpose, the IR transients at 1710 cm^{-1}, 1594 cm^{-1}, and 1238 cm^{-1} were quantitatively evaluated. Their average bleach recovery suggests a quantum yield for lumi-F formation of ~8%, which deviates from the reported value of 0.4% for the P_r formation (28). Note that the only scenario leading to an overestimation of the lumi-F quantum yield is an overlap of the (initial) bleach bands by short-lived absorption bands directly after photoexcitation. This can be excluded for all but the 1710 cm^{-1} bleach bands, and is thus very implausible to cause an error of one order of magnitude.

DISCUSSION

The analysis of the ultrafast data allows the construction of several reaction schemes for the primary processes, three of which (Schemes A–C, see Fig. 8) are taken into consideration, with Scheme C being discussed in more detail. In the following, τ_i and τ_{Vi} are used as given above.

Scheme *A* includes a structural relaxation from the Franck-Condon region to a S_1-state P^*_{fr} within τ_1, where a branching occurs. The productive pathway of the branching leads directly to the first metastable photoproduct lumi-F, whereas

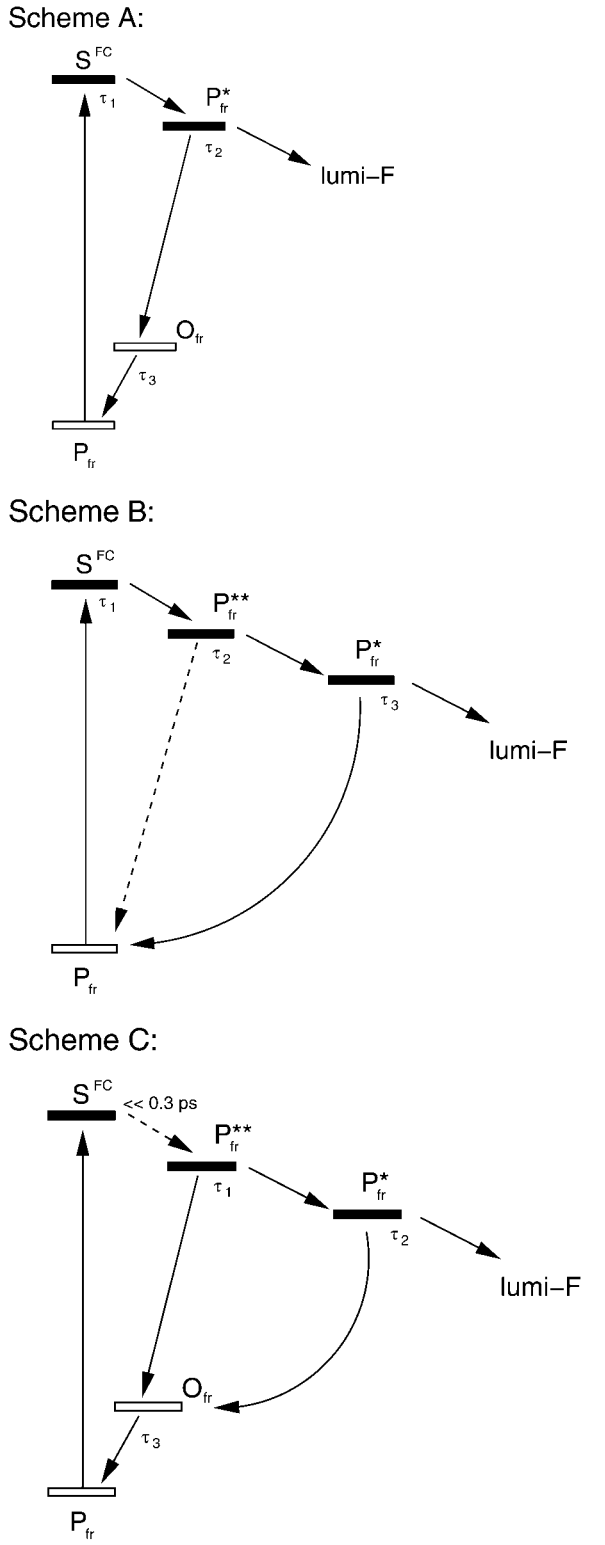

FIGURE 8 Reaction schemes for the P_{fr} primary reaction of Agp1-BV (see text). Solid bars denote excited electronic states, open bars denote electronic ground states.

the nonproductive part decays back to a vibrationally hot electronic ground-state O_{fr}, which repopulates the (cold) P_{fr} vibrational ground state. The decay of P_{fr}^{*} is supposed to occur with a rate constant of $1/\tau_2$ and the $O_{fr} \rightarrow P_{fr}$ transition with a rate of $1/\tau_3$. This reaction scheme is compatible with the analysis of the infrared data in that the positive contributions in A_3, which we attribute to a population of O_{fr}, always coincide spectrally with negative contributions from A_1 and A_2. Since the rate constants attributed to A_1 and A_2 are relatively similar, these two processes cannot be viewed as completely decoupled, hence the formation of O_{fr} shows kinetic contributions from the decay of S^{FC} and P_{fr}^{*}.

The deficiencies of Scheme A are twofold: Firstly, for the photoreaction to occur on an ultrafast timescale, one would assume the gradient of the S_1 surface in the Franck-Condon region to be relatively large. This implies that the initial structural relaxation (not necessarily along the $C_{15} = C_{16}$ torsional coordinate) occurs significantly faster than the system response time of the experiment and also faster than τ_1. Secondly, the decay of the excited-state absorption as detected in the VIS-VIS experiment shows τ_{V1} as dominant time constant, which is very close to τ_1. Thus, we can assume τ_1 to represent the dominant S_1 decay process, which contradicts its interpretation as movement out of the Franck-Condon region.

Scheme B is considered as a sequential reaction on the S_1 excited-state potential energy surface involving two S_1 substates, P_{fr}^{**} and P_{fr}^{*}. From the Franck-Condon region, the reaction proceeds via P_{fr}^{**} and P_{fr}^{*}, with a branching to lumi-F and to the electronic ground-state P_{fr} (in its vibrational ground state) that occurs with the decay of P_{fr}^{*}. Here, the time constants are assigned as follows: Relaxation from the Franck-Condon region with τ_1, reaction from P_{fr}^{**} to P_{fr}^{*} with τ_2, decay of P_{fr}^{*} and formation of lumi-F and P_{fr} with τ_3. An additional reaction path between P_{fr}^{**} and P_{fr} cannot be excluded.

Scheme B not only suffers from the same deficiencies as described above for Scheme A. Additionally, it cannot be assumed in general that the decay of the excited electronic-state P_{fr}^{*} leads directly to a (vibrationally) relaxed electronic ground state. For this unrelaxed ground state not to be traceable in the time-resolved infrared data, either its lifetime has to be small compared to τ_3, or its vibrational spectrum has to coincide with that of P_{fr}^{*} or of P_{fr}. However, the lifetime of the vibrationally excited electronic ground state can be estimated to ~3–4 ps by comparison to the P_r reaction (24). Further, since the additional state is assumed to be structurally or vibrationally unrelaxed, its spectrum cannot coincide with that of P_{fr}, and a coincidence with the P_{fr}^{*} vibrational spectrum seems far-fetched.

Scheme C accommodates our observations much better and avoids the difficulties of Schemes A and B. Here, the step from the Franck-Condon region to P_{fr}^{**} is assumed to be much faster than the system response time of the experiment and thus undetectable. With the decay of P_{fr}^{**}, a first branching occurs with reactions to P_{fr}^{*} and to the vibrationally unrelaxed electronic ground-state O_{fr}. The time constant τ_1 is assigned to the decay of P_{fr}^{**}. P_{fr}^{*}, with a lifetime of τ_2, decays with a branching between the formation of the first metastable photoproduct lumi-F and the formation of a structurally unrelaxed form of the educt-state P_{fr}, subsumed with O_{fr}. O_{fr} reacts back to the vibrational ground-state P_{fr}, via vibrational cooling and structural relaxation within τ_3. Since O_{fr} is populated from P_{fr}^{**} and P_{fr}^{*}, it is suggested to comprise vibrationally hot as well as structurally unrelaxed P_{fr} ground states that cannot be spectrally separated and share closely similar kinetics in their relaxation to P_{fr}.

It should be pointed out that the construction of the reaction schemes is based on the three time constants and the related DAS that were derived from the highly structured IR data. The two time constants of the VIS transients are nevertheless consistent with the dynamics described in Scheme C. Apparently the fit cannot distinguish between τ_1 and τ_2, but yields a weighted average τ_{V1}. This can be rationalized by the fact that the electronic absorption spectra are generally broad and unstructured, in contrast to vibrational spectra. Thus, the differences between the P_{fr}^{**} and the P_{fr}^{*} VIS spectra along with their similar lifetimes do not allow their separation into two kinetic components. The longer lifetime $\tau_{V2} = 3.3$ ps is in fair accordance with $\tau_3 = 4.0$ ps obtained in the IR. Following Scheme C, τ_{V2} has then to be attributed to processes on the electronic ground-state surface: 1), the recovery of the vibrationally fully relaxed P_{fr} electronic ground state, monitored at 755 nm; and 2), the decay of the structurally unrelaxed fraction of O_{fr}, which is suggested to contribute significantly to the transient absorbance at 630 nm.

Similar time constants have been observed in previous VIS-VIS experiments on the P_{fr} form of PhyA-PΦB (17) (0.68 ps and 4.0 ps) and the P_{fr} form of Cph1-PCB (18) (0.54 ps and 3.2 ps). These results suggested a reaction with two consecutive steps, but no specific reaction schemes were presented. For PhyA-PΦB, it remained unclear whether the longer time constant describes an electronic ground- or excited-state process. Similarly, the Cph1-PCB data did not allow an unequivocal assignment of the kinetics to electronic ground- or excited-state dynamics.

So far in this discussion, photoinduced intramolecular processes as transitions between different electronic-state potential energy surfaces, and conformational changes as well as vibrational relaxation of the chromophore, have been addressed. In addition, intermolecular energy flow from the chromophore to the surrounding protein and finally to the buffer solution will lead to an increased temperature of the microscopic sample volume. Timescales for energy conduction and heat diffusion, respectively, through protein matrices, have been found to be on the timescale of our experiment, e.g., 7–20 ps for hemoglobin (45). One temperature effect could be a change in the absorption bands of the surrounding water, leading to a spectrally rather unspecific baseline shift. This was not observed in our experiments.

Spectrally specific contributions could originate from heating of the protein backbone, which for bacteriorhodopsin have been shown to yield IR difference bands in the amide II region at ~1550 cm^{-1} and (much smaller) in the amide I region (46). The difference signals for long times (A_0 spectrum) do not give indications for such bands. Further spectrally specific changes at long delay times (e.g., 50 ps) could be due to the vibrational spectrum of the chromophore, having released its excess energy to the environment. However, the band shift induced by such a small temperature change (a few Kelvin) is negligible, considering the relatively low chromophore concentration (41,46). We therefore conclude that neither the determination of the quantum yield nor the observability of the lumi-F state are affected by a temperature effect.

The identification of A_3 (and thus also of τ_3) as a relaxation process of a vibrationally unrelaxed P_{fr} electronic ground state leads to the conclusion that the first metastable photoproduct, which we assume to be lumi-F, can only be populated from the longest living electronic excited-state P_{fr}^*, which decays within $\tau_2 = 1.3$ ps. Considering the low quantum yield of the lumi-F formation, the fact that the cooling process is readily observed strongly suggests it to be part of the nonproductive pathway. Thus, an involvement of τ_3 in the isomerization reaction is very unlikely. Although the low quantum yield does not allow the detection of lumi-F product bands, this suggests the *E-Z* isomerization to occur along the excited-state reaction pathway, with an upper limit for the isomerization time of $\tau_2 = 1.3$ ps. A stepwise isomerization via a ground-state reaction is implausible, since time-resolved experiments on the P_{fr} state of other phytochromes (17,18) with higher isomerization quantum yields were also unable to detect spectral changes beyond the order of magnitude of τ_3.

The isomerization quantum yield of the P_{fr} primary reaction, as derived here via the primary recovery of the P_{fr} educt-state, is very similar to that of the P_r reaction (24). In contrast to the P_r reaction, where the yield of the primary reaction (lumi-R formation) was found to be equal to that of the P_{fr} formation (28), the corresponding values of the P_{fr} reaction differ in more than one order of magnitude, i.e., 8% vs. 0.4%. This suggests the possibility of a short-cut reaction originating in an intermediate state along the $P_{fr} \rightarrow P_r$ reaction path and leading back to the P_{fr} form. In consequence, this dark reaction would have to include a thermally driven *Z-E* isomerization. Double-bond isomerizations of free chromophores often require the energy of an absorbed photon (47,48). Thus, such a short-cut reaction was unexpected. However, dark conversion of, e.g., bacteriorhodopsin (49), PYP (50), or phytochromes (28) are examples for thermally driven isomerization reactions that take place within the protein environment. The dark conversion of *Agrobacterium* phytochrome Agp2 and some other bacterial phytochromes proceeds from P_r to P_{fr} (51,52). These examples show that also a $Z \rightarrow E$ dark isomerization around the $C_{15} = C_{16}$ double bond of the bilin chromophore is not impossible. This study suggests that such a dark isomerization is an integral part of the Agp1 photocycle. It seems that Agp1 is an exception in this respect, because the overall quantum yield of the P_{fr}-to-P_r conversion of other phytochromes is >10% and thus in the range of the P_{fr} to lumi-F quantum yield estimated here (28). The rather complex P_{fr}-to-P_r reaction of Agp1 is thus most likely the consequence of an evolutionary process which finally resulted in the rather low P_{fr}-to-P_r quantum yield of this phytochrome.

Comparison of reaction Scheme C of the P_{fr} primary reaction (Fig. 8) with the scheme of the P_r primary reaction (24) yields close similarities. The schemes for both reactions are basically identical, with the only difference in the values of the time constants. The decay of the first structurally relaxed excited electronic-state, P_{fr}^{**} in the P_{fr} scheme and A in the P_r scheme, with 0.3 and 0.7 ps, respectively, and the relaxation on the electronic ground state, i.e., the decay of O_{fr} and O_r, with 4.0 and 3.3 ps, respectively, show very similar time constants. In contrast, the lifetime of the longest-lived S_1 species differs significantly from 1.3 ps in the P_{fr} reaction to 33.3 ps in the P_r reaction. The very short S_1 lifetime in the P_{fr} reaction is consistent with the vanishingly small fluorescence quantum yield of the P_{fr} reaction as compared to the P_r reaction (26). Note that the similarity of the reaction schemes for P_r and P_{fr} implies in turn specific similarities of the two sets of DAS—A_i (P_r) (24) and A_i (P_{fr}). In fact, qualitative match is found concerning their sign and relative spectral position. Observed differences, e.g., in terms of spectral width and absolute spectral position are not unexpected, since both reactions originate from different chromophore configurations and thus exhibit different ground- and excited-state vibrational spectra.

The observation of a slow P_r reaction and a fast P_{fr} reaction in Agp1-BV is in line with earlier results on the primary photoreactions of different phytochromes (16–18). Similarly distinct timescales for the forward- and backward-direction of *cis-trans* isomerizations have been found in the photochemistry of stilbene and azobenzene. In azobenzene, the isomerization processes are completed within 10 ps for the *trans-cis* and within 1 ps for the *cis-trans* direction (53). In stilbene, the *cis-trans* isomerization takes <1 ps and the *trans-cis* isomerization >10 ps, dependent on the solvent (54). The asymmetry of the reaction kinetics with respect to the initial configuration reflects the differently shaped regions of the excited-state potential energy surfaces that are accessed upon photoexcitation of the respective *cis*- or *trans*-state. Certainly, fundamental aspects of *cis-trans* photoisomerization already discussed for stilbene and azobenzene in solution can be applied to bilin chromophores in a protein environment. However, the example of retinal proteins (55,56) demonstrates how drastically the specific properties of the strongly anisotropic environment realized by the protein moiety can alter the photoinduced isomerization kinetics of a protein-bound chromophore.

In conclusion, femtosecond IR spectroscopy has brought forward a new and more specified reaction scheme of the P_{fr} photoisomerization of Agp1-BV. Whether or not a unique reaction scheme applies to the P_{fr} reaction of many phytochromes, if not of phytochromes in general, is up to future studies.

The authors thank Peter Hildebrandt and Maria Andrea Mroginski for helpful discussion.

C.S., M.M.N.W., and R.D. acknowledge support by Deutsche Forschungsgemeinschaft, Forschungsschwerpunkt ''Optische Technologien und lasergesteuerte Prozesse'' Rheinland-Pfalz, and Stiftung Rheinland-Pfalz für Innovation. R.G. was supported by Deutsche Forschungsgemeinschaft Graduiertenkolleg grant No. 792, and T.L. and N.M. by Deutsche Forschungsgemeinschaft grant No. Sfb 498, B2.

REFERENCES

1. Lamparter, T. 2004. Evolution of cyanobacterial and plant phytochromes. *FEBS Lett.* 573:1–5.
2. Rockwell, N. C., Y.-S. Su, and J. C. Lagarias. 2006. Phytochrome structure and signaling mechanisms. *Annu. Rev. Plant Biol.* 57:837–858.
3. Wagner, J. R., J. S. Brunzelle, K. T. Forest, and R. D. Vierstra. 2005. A light-sensing knot revealed by the structure of the chromophore-binding domain of phytochrome. *Nature.* 438:325–331.
4. Wagner, J. R., J. Zhang, J. S. Brunzelle, R. D. Vierstra, and K. T. Forest. 2007. High resolution structure of *Deinococcu*s bacteriophytochrome yields new insights into phytochrome architecture and evolution. *J. Biol. Chem.* 282:12298–12309.
5. Yang, X., E. A. Stojkovic, J. Kuk, and K. Moffat. 2007. Crystal structure of the chromophore binding domain of an unusual bacteriophytochrome, RpBphP3, reveals residues that modulate photoconversion. *Proc. Natl. Acad. Sci. USA.* 104:12571–12576.
6. Rüdiger, W., F. Thümmler, E. Cmiel, and S. Schneider. 1983. Chromophore structure of the physiologically active form (P_{fr}) of phytochrome. *Proc. Natl. Acad. Sci. USA.* 80:6244–6248.
7. Mroginski, M. A., D. H. Murgida, D. von Stetten, C. Kneip, F. Mark, and P. Hildebrandt. 2004. Determination of the chromophore structures in the photoinduced reaction cycle of phytochrome. *J. Am. Chem. Soc.* 126:16734–16735.
8. Eilfeld, P., and W. Rüdiger. 2007. Absorption spectra of phytochrome intermediates. *Z. Naturforsch.* [*C*]. 40:109–114.
9. Foerstendorf, H., E. Mummert, E. Schäfer, H. Scheer, and F. Siebert. 1996. Fourier-transform infrared spectroscopy of phytochrome: difference spectra of the intermediates of the photoreactions. *Biochemistry.* 35:10793–10799.
10. Foerstendorf, H., C. Benda, W. Gärtner, M. Storf, H. Scheer, and F. Siebert. 2001. FTIR studies of phytochrome photoreactions reveal the C=O bands of the chromophore: consequences for its protonations states, conformation, and protein interaction. *Biochemistry.* 40:14952–14959.
11. Matysik, J., P. Hildebrandt, W. Schlamann, S. E. Braslavsky, and K. Schaffner. 1995. Fourier-transform resonance Raman spectroscopy of intermediates of the phytochrome photocycle. *Biochemistry.* 34:10497–10507.
12. Andel III, F., J. C. Lagarias, and R. A. Mathies. 1996. Resonance Raman analysis of chromophore structure in the lumi-R photoproduct of phytochrome. *Biochemistry.* 35:15997–16008.
13. Kneip, C., D. Mozley, P. Hildebrandt, W. Gärtner, S. E. Braslavsky, and K. Schaffner. 1997. Effect of chromophore exchange on the resonance Raman spectra of recombinant phytochromes. *FEBS Lett.* 414: 23–26.
14. Remberg, A., I. Lindner, T. Lamparter, J. Hughes, C. Kneip, P. Hildebrandt, S. E. Braslavsky, W. Gärtner, and K. Schaffner. 1997. Raman-spectroscopic and light-induced kinetic characterization of a recombinant phytochrome of the cyanobacterium *Synechocystis*. *Biochemistry.* 36:13389–13395.
15. von Stetten, D., S. Seibeck, N. Michael, P. Scheerer, M. A. Mroginski, D. H. Murgida, N. Krauss, M. P. Heyn, P. Hildebrandt, B. Borucki, and T. Lamparter. 2007. Highly conserved residues Asp-197 and His-250 in Agp1 phytochrome control the proton affinity of the chromophore and P_{fr} formation. *J. Biol. Chem.* 282:2116–2123.
16. Bischoff, M., G. Hermann, S. Rentsch, and D. Strehlow. 1998. Ultrashort processes of native phytochrome: femtosecond kinetics of the far-red-absorbing form P_{fr}. *J. Phys. Chem. A.* 102:4399–4404.
17. Bischoff, M., G. Hermann, S. Rentsch, and D. Strehlow. 2001. First steps in the phytochrome phototransformation: a comparative femtosecond study on the forward ($P_r \rightarrow P_{fr}$) and back reaction ($P_{fr} \rightarrow P_r$). *Biochemistry.* 40:181–186.
18. Heyne, K., J. Herbst, D. Stehlik, B. Esteban, T. Lamparter, J. Hughes, and R. Diller. 2002. Ultrafast dynamics of phytochrome from the cyanobacterium *Synechocystis*, reconstituted with phycocyanobilin and phycoerythrobilin. *Biophys. J.* 82:1004–1016.
19. Kandori, H., K. Yoshihara, and S. Tokutomi. 1992. Primary process of phytochrome: initial step of photomorphogenesis in green plants. *J. Am. Chem. Soc.* 114:10958–10959.
20. Bischoff, M., G. Hermann, S. Rentsch, D. Strehlow, S. Winter, and H. Chosrowjan. 2000. Excited-state processes in phycocyanobilin studied by femtosecond spectroscopy. *J. Phys. Chem. B.* 104:1810–1816.
21. Rentsch, S., M. Bischoff, G. Hermann, and D. Strehlow. 1998. Fs spectroscopic studies of the plant photoreceptor phytochrome. *Appl. Phys. B.* 66:259–261.
22. Andel III, F., K. C. Hasson, F. Gai, P. A. Anfinrud, and R. A. Mathies. 1997. Femtosecond time-resolved spectroscopy of the primary photochemistry of phytochrome. *Biospectroscopy.* 3:421–433.
23. van Thor, J. J., K. L. Ronayne, and M. Towrie. 2007. Formation of the early photoproduct lumi-R of cyanobacterial phytochrome Cph1 observed by ultrafast mid-infrared spectroscopy. *J. Am. Chem. Soc.* 129:126–132.
24. Schumann, C., R. Groß, N. Michael, T. Lamparter, and R. Diller. 2007. Sub-Picosecond mid-infrared spectroscopy of phytochrome Agp1 from *Agrobacterium tumefaciens*. *ChemPhysChem.* 11:1657–1663.
25. Holzwarth, A. R., J. Wendler, B. P. Ruzsicska, S. E. Braslavsky, and K. Schaffner. 1984. Picosecond time-resolved and stationary fluorescence of oat phytochrome highly enriched in the native 124 kDa Protein. *Biochim. Biophys. Acta.* 791:265–273.
26. Wendler, J., A. R. Holzwarth, S. E. Braslavsky, and K. Schaffner. 1984. Wavelength-resolved fluorescence decay and fluorescence quantum yield of large phytochrome from oat shoots. *Biochim. Biophys. Acta.* 786:213–221.
27. Holzwarth, A. R., E. Venuti, S. E. Braslavsky, and K. Schaffner. 1992. The phototransformation process in phytochrome: I. Ultrafast fluorescence component and kinetic models for the initial $P_r \rightarrow P_{fr}$ transformation steps in native phytochrome. *Biochim. Biophys. Acta.* 1140: 59–68.
28. Lamparter, T., N. Michael, F. Mittmann, and B. Esteban. 2002. Phytochrome from *Agrobacterium tumefaciens* has unusual spectral properties and reveals an N-terminal chromophore attachment site. *Proc. Natl. Acad. Sci. USA.* 99:11628–11633.
29. Lamparter, T., M. Carrascal, N. Michael, E. Martinez, G. Rottwinkel, and J. Abian. 2004. The biliverdin chromophore binds covalently to a conserved cysteine residue in the N-terminus of *Agrobacterium* phytochrome Agp1. *Biochemistry.* 43:3659–3669.
30. Borucki, B., D. v. Stetten, S. Seibeck, T. Lamparter, N. Michael, M. A. Mroginski, H. Otto, D. H. Murgida, M. P. Heyn, and P. Hildebrandt. 2005. Light-induced proton release of phytochrome is coupled to the transient deprotonation of the tetrapyrrole chromophore. *J. Biol. Chem.* 280:34358–34364.
31. Inomata, K., M. A. S. Hammam, H. Kinoshita, Y. Murata, H. Khawn, S. Noack, N. Michael, and T. Lamparter. 2005. Sterically locked

synthetic bilin derivates and phytochrome Agp1 from *Agrobacterium tumefaciens* form photoinsensitive P_r- and P_{fr}-like adducts. *J. Biol. Chem.* 280:24491–24497.

32. Inomata, K., S. Noack, M. A. S. Hammam, H. Khawn, H. Kinoshita, Y. Murata, N. Michael, P. Scheerer, N. Krauss, and T. Lamparter. 2006. Assembly of synthetic locked chromophores with *Agrobacterium* phytochromes Agp1 and Agp2. *J. Biol. Chem.* 281:28162–28173.
33. Reference deleted in proof.
34. Herbst, J., K. Heyne, and R. Diller. 2002. Femtosecond infrared spectroscopy of bacteriorhodopsin chromophore isomerization. *Science.* 297:822–825.
35. Diller, R., R. Jakober, C. Schumann, F. Peters, J. P. Klare, and M. Engelhard. 2006. The *trans-cis* isomerization reaction dynamics in sensory rhodopsin II by femtosecond time-resolved midinfrared spectroscopy: chromophore and protein dynamics. *Biopolymers.* 82:358–362.
36. Peters, F., J. Herbst, J. Tittor, D. Oesterhelt, and R. Diller. 2006. Primary reaction dynamics of halorhodopsin, observed by subpicosecond IR-vibrational spectroscopy. *Chem. Phys.* 323:109–116.
37. Lochbrunner, S., P. Huppmann, and E. Riedle. 2000. Cross-correlation measurements of ultrashort visible pulses: comparison between nonlinear crystals and SiC photodiodes. *Opt. Commun.* 184:321–328.
38. Frisch, M. J., G. W. Trucks, H. B. Schlegel, G. E. Scuseria, M. A. Robb, J. R. Cheeseman, J. A. Montgomery, Jr., T. Vreven, K. N. Kudin, J. C. Burant, J. M. Millam, S. S. Iyengar, J. Tomasi, V. Barone, B. Mennucci, M. Cossi, G. Scalmani, N. Rega, G. A. Petersson, H. Nakatsuji, M. Hada, M. Ehara, K. Toyota, R. Fukuda, J. Hasegawa, M. Ishida, T. Nakajima, Y. Honda, O. Kitao, H. Nakai, M. Klene, X. Li, J. E. Knox, H. P. Hratchian, J. B. Cross, V. Bakken, C. Adamo, J. Jaramillo, R. Gomperts, R. E. Stratmann, O. Yazyev, A. J. Austin, R. Cammi, C. Pomelli, J. W. Ochterski, P. Y. Ayala, K. Morokuma, G. A. Voth, P. Salvador, J. J. Dannenberg, V. G. Zakrzewski, S. Dapprich, A. D. Daniels, M. C. Strain, O. Farkas, D. K. Malick, A. D. Rabuck, K. Raghavachari, J. B. Foresman, J. V. Ortiz, Q. Cui, A. G. Baboul, S. Clifford, J. Cioslowski, B. B. Stefanov, G. Liu, A. Liashenko, P. Piskorz, I. Komaromi, R. L. Martin, D. J. Fox, T. Keith, M. A. Al-Laham, C. Y. Peng, A. Nanayakkara, M. Challacombe, P. M. W. Gill, B. Johnson, W. Chen, M. W. Wong, C. Gonzalez, and J. A. Pople. 2004. Gaussian 03, Rev. C02. Gaussian, Wallingford, CT.
39. Wong, M. W. 1996. Vibrational frequency prediction using density functional theory. *Chem. Phys. Lett.* 256:391–399.
40. van Thor, J. J., N. Fisher, and P. R. Rich. 2005. Assignments of the P_{fr}-P_r FTIR difference spectrum of cyanobacteria phytochrome Cph1 using ^{15}N and ^{13}C isotopically labeled phycocyanobilin chromophore. *J. Phys. Chem. B.* 109:20597–20604.
41. Hamm, P., S. M. Ohline, and W. Zinth. 1997. Vibrational cooling after ultrafast photoisomerization of azobenzene measured by femtosecond infrared spectroscopy. *J. Chem. Phys.* 106:519–529.
42. Hamm, P., M. Zurek, T. Roschinger, H. Patzelt, D. Oesterhelt, and W. Zinth. 1997. Subpicosecond infrared spectroscopy on the photoisomerization of the protonated Schiff base of all-*trans* retinal. *Chem. Phys. Lett.* 268:180–186.
43. Owrutsky, J., D. Raftery, and R. Hochstrasser. 1994. Vibrational relaxation dynamics in solutions. *Annu. Rev. Phys. Chem.* 45:519–555.
44. Kim, J. E., and R. A. Mathies. 2002. Anti-Stokes Raman study of vibrational cooling dynamics in the primary photochemistry of rhodopsin. *J. Phys. Chem. A.* 106:8508–8515.
45. Lian, T., B. Locke, Y. Kholodenko, and R. Hochstrasser. 1994. Energy flow from solute to solvent probed by femtosecond IR spectroscopy: malachite green and heme protein solutions. *J. Phys. Chem.* 98:11648–11656.
46. Rödig, C., H. Georg, F. Siebert, I. Rousso, and M. Sheves. 1999. Temperature effects of excitation laser pulses during step-scan FTIR measurements. *Laser Chem.* 19:169–172.
47. Rentsch, S., G. Hermann, M. Bischoff, D. Strehlow, and M. Rentsch. 1997. Femtosecond spectroscopic studies on the red light-absorbing form of oat phytochrome and 2,3-dihydrobiliverdin. *Photochem. Photobiol.* 66:585–590.
48. Lamparter, T., and N. Michael. 2005. Agrobacterium phytochrome as an enzyme for the production of ZZE bilins. *Biochemistry.* 44:8461–8469.
49. Oesterhelt, D., and J. Tittor. 1989. Two pumps, one principle: light-driven ion transport in *Halobacteria. Trends Biochem. Sci.* 14:57–61.
50. Meyer, T. E., S. Devanathan, T. Woo, E. D. Getzoff, G. Tollin, and M. A. Cusanovich. 2003. Site-specific mutations provide new insights into the origin of pH effects and alternative spectral forms in the photoactive yellow protein from *Halorhodospira halophila. Biochemistry.* 42:3319–3325.
51. Giraud, E., J. Fardoux, N. Fourrier, L. Hannibal, B. Genty, P. Bouyer, B. Dreyfus, and A. Vermeglio. 2002. Bacteriophytochrome controls photosystem synthesis in anoxygenic bacteria. *Nature.* 417:202–205.
52. Karniol, B., and R. Vierstra. 2003. The pair of bacteriophytochromes from *Agrobacterium tumefaciens* are histidine kinases with opposing photobiological properties. *Proc. Natl. Acad. Sci. USA.* 100:2807–2812.
53. Satzger, H., C. Root, C. Renner, R. Behrendt, L. Moroder, J. Wachtveitl, and W. Zinth. 2004. Picosecond dynamics in water-soluble azobenzene-peptides. *Chem. Phys. Lett.* 396:191–197.
54. Sension, R., S. Repinec, A. Szarka, and R. Hochstrasser. 1993. Femtosecond laser studies of the *cis*-stilbene photoisomerization reactions. *J. Chem. Phys.* 98:6291–6315.
55. Song, L., M. El-Sayed, and J. Lanyi. 1993. Protein catalysis of the retinal subpicosecond photoisomerization in the primary process of bacteriorhodopsin photosynthesis. *Science.* 261:891–894.
56. Heyne, K., J. Herbst, B. Dominguez-Herradon, U. Alexiev, and R. Diller. 2000. Reaction control in bacteriorhodopsin: impact of Arg^{82} and Asp^{85} on the fast retinal isomerization, studied in the second site revertant $Arg^{82}Ala/Gly^{231}Cys$ and various purple and blue forms of bacteriorhodopsin. *J. Phys. Chem. B.* 104:6053–6058.
57. Hamm, P. 1995. Coherent effects in femtosecond infrared spectroscopy. *Chem. Phys.* 200:415–429.
58. Kovalenko, S. A., A. L. Dobryakov, J. Ruthmann, and N. P. Ernsting. 1999. Femtosecond spectroscopy of condensed phases with chirped supercontinuum probing. *Phys. Rev. A.* 59:2369–2384.